J. Fluid Mech. (1991), *vol.* 222, *pp.* 665–691
Printed in Great Britain

Long waves on inclined films at high Reynolds number

By TH. PROKOPIOU, M. CHENG AND H.-C. CHANG
Department of Chemical Engineering, University of Notre Dame, Notre Dame, IN 46556, USA

(Received 7 August 1989 and in revised form 5 June 1990)

At large Reynolds number ($Re > 10$), waves on inclined films grow rapidly downstream in both amplitude and wavelength to the extent that linear stability theory cannot adequately describe their velocity–wavenumber relationship. The wavelength increases indefinitely until solitary waves are formed very far downstream. In a recent experiment of Brauner & Maron (1982), this evolution to long waves is observed to occur by successive wavelength doubling. In this analysis, we develop a second-order integral boundary-layer approximation for long waves at intermediate Re of $O(\epsilon^{-1})$, where ϵ is the dimensionless wavenumber scaled with respect to the film thickness. (A second-order theory is needed because it introduces important dissipation terms which allow periodic and solitary waveforms to exist when surface tension is negligible.) After showing that this model can adequately describe infinitesimal waves at inception, we verify the existence of solitary waves and long-wavelength periodic waves near the critical Reynolds number with a weakly nonlinear analysis. These finite-amplitude waves are then numerically continued into the more important high-Re and strongly nonlinear regions. It is shown that the solitary wave speed approaches 1.67 times the Nusselt velocity, and the thickness of the substrate film approaches 0.47 times the Nusselt film thickness at large Re. These results are favourably compared to experimental data of Chu & Dukler (1974, 1975). We also confirm the period-doubling scenario of Brauner & Maron by showing that short finite-amplitude monochromatic waves are unstable to subharmonic instability.

1. Introduction

The stability of vertical and inclined films has traditionally been studied by a linear Orr–Sommerfeld analysis (see the review by Lin 1983). While linear stability theory gives a reasonably accurate prediction of the critical conditions for the onset of waves, it is inadequate for developed finite-amplitude waves far downstream from the feed. Recent experiments by Alekseenko, Nakoryakov & Pokusaev (1985) and Brauner & Maron (1982) indicate that waves at inception near the entry are indeed well described by the linear theory. However, for conditions far from criticality where the linear growth rate is significant, these waves quickly grow in amplitude and wavelength as they travel downstream. Their content of Fourier modes also increases significantly until the waves become strongly asymmetric. Beyond an entry length of about 500 times the Nusselt film thickness, $h_N = (3\,\nu Q/g\,cos\theta)^{\frac{1}{3}}$, where Q is the flow rate per unit span width and θ is the inclination angle from vertical, the waves reach a permanent form and travel downstream without discernible changes in speed and shape. Moreover, if the Reynolds number, $Re = u_N h_N/\nu$ (where $u_N = Q/h_N = g\cos\theta h_N^2/3\nu$ is the Nusselt velocity for the average velocity of a flat film),

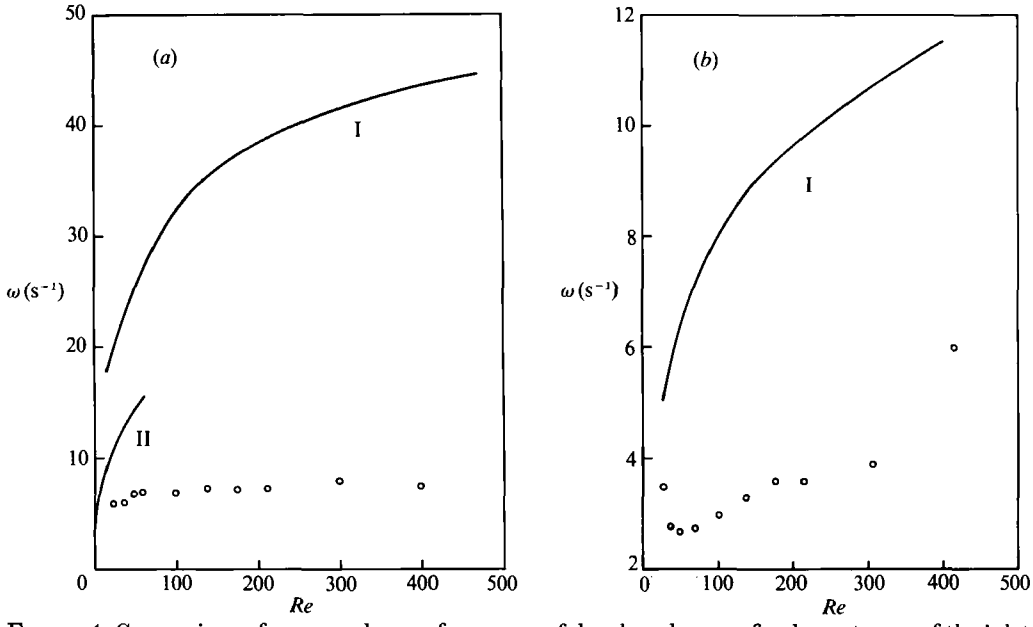

FIGURE 1. Comparison of measured wave frequency of developed waves far downstream of the inlet by Brauner & Maron for water (○) to Yih's low-Re theory (II) and our integral boundary-layer theory (I) for the maximum-growing linear mode. The inclination angles are (*a*) $\theta = 51°$ and (*b*) $\theta = 84°$. The more horizontal inclination has a lower growth rate and has not evolved to the same extent.

is smaller than 50 for vertical films to 500 for almost horizontal films, the waves remain approximately two-dimensional without much undulation in the cross-stream direction. That these developed waves cannot be described by linear stability theory is shown in figure 1 where Brauner & Maron's measured wave frequency for developed waves at 51° and 84° from vertical is compared to linear predictions of the wave frequency for the maximum-growing linear mode. The theoretical curves include our linear stability theory for intermediate Reynolds number, which will be developed in the next section, and Yih's (1963) long-wave Orr–Sommerfeld result for small Reynolds numbers. Yih's theory predicts that the maximum-growing linear mode of a vertical film has a leading-order dimensionless frequency of $k_m c_m/2\pi$, where k_m and c_m are the maximum-growing wavenumber and its linear phase velocity:

$$k_m = [2(Re - \tfrac{5}{6}\tan\theta)/5\Sigma]^{\frac{1}{2}},$$

$$c_m = 3 - [3 + \tfrac{12}{7}Re(Re - \tfrac{5}{6}\tan\theta)]\,k_m^2;$$

$$\Sigma = \tfrac{2}{9}We\,Re - \tfrac{6}{5}\tan\theta + \tfrac{471}{112}Re + \tfrac{4}{15}Re\tan^2\theta - \tfrac{34726}{17325}Re^2\tan\theta + \tfrac{151744}{75075}Re^3,$$

and the Weber number We is defined as $\sigma/\rho u_N^2 h_N$. (Note that Yih used the interfacial velocity as the characteristic velocity and his Weber number is also defined differently.) An order of magnitude discrepancy between data and theory is evident for some of the experimental conditions. Waves on the more horizontal incline, because of their smaller growth rate, do not evolve as much within the channel and have wave frequencies closer to the linear waves. Note that the developed waves can also be excited by pulsing the feed rate. These artificially excited waves reach their permanent form immediately without an entry region. Alekseenko *et al.* do not observe any difference between the naturally and artificially excited finite-amplitude waves. It is interesting to note how the naturally excited waves which grow from

infinitesimal waves, evolve from the entry. Figure 9 of Brauner & Maron's (1982) paper presents the wave spectra for $Re = 144$ and $\theta = 60°$ at various locations downstream. (Actually, the spectra of the mass transfer rate of a chemical species from the liquid to the solid bottom are measured. However, Brauner & Maron have experimentally demonstrated that these spectra are close to the wave spectra.) Near the entry, the small-amplitude waves show a maximum in their spectrum at 10 Hz which is close to the wave frequency of the linear maximum growing mode. However, the energy of the waves seems to shift to its subharmonic at 5 Hz and lower frequencies further downstream. This 'period-doubling' phenomenon occurs again downstream until a 2.5 Hz frequency begins to dominate the spectrum of developed waves near the exit of their channel. The same phenomenon has also been observed by Choi (1977) in his experiments on sheared deep-water waves.

For Reynolds numbers of order unity with respect to the parameter $\epsilon = h_N/L$, where L is the characteristic length in the flow direction which is typically taken to be the wavelength of the waves such that ϵ is the dimensionless wavenumber, finite-amplitude waves have been studied by Benney (1966), Lin (1969), Gjevik (1970) and Nakaya (1975). They generally carried out a weakly nonlinear analysis of the system near the neutral curve where monochromatic linear waves have zero growth rates. Also, only fundamental modes with small growth rates and, in certain cases, their first superharmonics are considered in deriving the Stuart–Landau equation for the amplitude of the wave. In a recent paper, Chang (1989) has demonstrated that the weakly nonlinear problem can yield finite-amplitude waves which contain many Fourier modes. This includes a solitary wave with a broad and continuous Fourier spectrum. These solitary waves have been numerically constructed by Pumir, Manneville & Pomeau (1983) and Nakaya (1989). Nakaya has proposed that even seemingly periodic interfacial waves are actually trains of equally spaced solitary waves.

For intermediate Reynolds numbers of $O(\epsilon^{-1})$, nonlinear analyses have been carried out by Shkadov (1967, 1968) and Lee (1969) who again considered only the first two harmonics of a periodic wave with small linear growth rates. To study strongly nonlinear waves with large mode content, it is extremely difficult to tackle the complete equations of motion and the complex free-surface conditions. Instead, a long-wave expansion in ϵ can be carried out to derive a much simpler evolution equation for the interface. For Reynolds number of order unity, as mentioned above, this expansion can be carried out formally (Benney 1966). Unfortunately, for intermediate Reynolds number of $O(\epsilon^{-1})$, an approximate Kármán–Polhausen integral boundary-layer theory must be introduced. In this formulation, a velocity profile is imposed *a priori* after expanding the Navier–Stokes equation to leading order in ϵ. The $O(\epsilon)$ expansion with a flat velocity profile is essentially the shallow-water theory of Dressler (1949) and Stoker (1957). A numerical study by Brock (1970) indicates that continuous finite-amplitude waveforms do not exist for Dressler's shallow-water equations. To remedy this, Needham & Merkin (1984) have added an empirical second-order dissipation term to Dressler's equation to model 'normal shear' and showed that periodic waveforms are now possible. Needham & Merkin (1986) and Hwang and Chang (1987) have shown that solitary waves with speeds close to $1.5u_N$ also exist for this modified shallow-water equation. However, the amplitudes of both the periodic and solitary waves are strongly dependent on an empirical viscosity parameter associated with the added dissipation term. Since this empirical viscosity is difficult to estimate, comparison against measured wave amplitudes and wavelengths is impossible. Recently, Alekseenko *et al.* (1985) have

imposed a parabolic velocity profile and derived an alternative evolution equation valid to $O(\epsilon)$. Their data for vertical films and Bertschy, Chin & Abernathy's (1983) measurements for inclined films indicate that this is a more appropriate profile for intermediate-Reynolds-number (< 1000) flow sufficiently far from the entry. Although Alekseenko *et al.* have shown that the linearized version of their evolution equation yields excellent prediction of small-amplitude waves near inception and near onset, they did not attempt to construct finite-amplitude waveforms from their nonlinear equations. As we shall demonstrate, their first-order theory still does not allow the construction of finite-amplitude periodic waves because the second-order dissipation term sought by Needham & Merkin (1986) remains absent when surface tension is negligible.

In this paper, we extend Alekseenko *et al.*'s integral boundary-layer theory to second order in ϵ. In this higher-order resolution, the normal shear contribution, which Needham & Merkin (1984) have attempted to model empirically, is explicitly derived from the equations of motion. We then show by a weakly nonlinear analysis near criticality that, under $O(\epsilon^2)$ resolution, periodic and solitary travelling waveforms are indeed solutions to the evolution equations. Our weakly nonlinear study includes a Melnikov analysis which yields a solitary wave and a family of periodic waves near onset. The waves close to the solitary waves contain a large number of Fourier modes which can never be modelled with a few harmonics. We also numerically continue these waveforms into the highly nonlinear and large-Reynolds-numbers region far away from criticality. It is shown by comparison to experimental data that the well-developed waves, such as the ones shown in figure 1, approach the solitary wave limit at large Reynolds number with wave frequencies much smaller than that corresponding to the linear maximum-growing mode. Since our theory does not involve any empirical terms, we are able to compare our results to experimental data and show favourable agreement. This construction does not reveal the stability of these waveforms although experimental data clearly show a gradual downstream evolution to longer waves until the solitary wave limit is approached. To remedy this, we also study the evolution to long waves, showing that short-wavelength periodic waves are unstable to subharmonic instability which is consistent with Brauner & Maron's (1982) experimental observation. The periodic waves are then sensitive to subharmonic disturbances, and a period-doubling cascade is an important component of the evolution to solitary waves.

2. Shallow-water theory and linear stability

Following integral boundary-layer theory, we shall derive the normally averaged evolution equations for the x-momentum and the kinematic condition. In this model, the y-momentum balance is assumed to be dominated by hydrostatic forces. Scaling the downstream coordinate x by the unknown wavelength L, the normal coordinate y by h_N, the x-component velocity by u_N, the y-component by $\epsilon\, u_N$, pressure by ρu_N^2 and time by L/u_N, the leading-order version of the equations of motion and the pertinent boundary conditions become

$$\frac{\partial u}{\partial t}+u\frac{\partial u}{\partial x}+v\frac{\partial u}{\partial y}=-\frac{\partial p}{\partial x}+\frac{Fr}{\epsilon}\cos\theta+\frac{1}{Re\,\epsilon}\left(\epsilon^2\frac{\partial^2 u}{\partial x^2}+\frac{\partial^2 u}{\partial y^2}\right), \tag{1}$$

$$\frac{\partial p}{\partial y}=-Fr\sin\theta, \tag{2}$$

continuity $$\frac{\partial u}{\partial x}+\frac{\partial v}{\partial y}=0, \tag{3}$$

no-slip $$y=0, \quad u=v=0, \tag{4}$$

kinematic condition $$y=h, \quad \frac{\partial h}{\partial t}=v-u\frac{\partial h}{\partial x}, \tag{5}$$

normal stress $$p_a-p+\frac{2\epsilon}{Re}\frac{\partial v}{\partial y}=We\,\epsilon^2 h_{xx}(1-\tfrac{3}{2}\epsilon^2 h_x^2), \tag{6}$$

tangential stress $$\frac{\partial u}{\partial y}+\epsilon^2\frac{\partial v}{\partial x}+4\epsilon^2\frac{\partial h}{\partial x}\frac{\partial v}{\partial y}=0, \tag{7}$$

where p_a is the constant air pressure and the following orders have been assigned to the parameters, corresponding to intermediate-Reynolds-number flow of common fluids:

$$Re=u_N h_N/\nu=O(\epsilon^{-1}), \tag{8}$$

$$We=\sigma/\rho u_N^2 h_N=(3^{\frac{1}{3}}Fi^{\frac{1}{3}})/(\mathrm{Re}^{\frac{5}{3}}\cos\theta^{\frac{1}{3}})=O(\epsilon^{-2}), \tag{9}$$

$$Fr=gh_N/u_N^2=O(\epsilon), \tag{10}$$

where We is the Weber number, $Fi=\sigma^3/\rho^3\,g\nu^4$ is the film number, which is independent of the flow conditions, and Fr is the Froude number. The approximate Kármán–Polhausen integral boundary-layer theory, which has been very successfully applied in airfoil analysis (von Kármán 1921; Batchelor 1967), will be applied to the above equations. The key approximation is the assumption of a velocity profile to allow integration of the equations in the y-direction. As we shall demonstrate in the Appendix, this approximation is most appropriate for $Re=O(\epsilon^{-1})$. We shall hence restrict ourselves to this order of Re. For low-Reynolds-number films, $Re=O(1)$, this *a priori* approximation of the velocity profile is not necessary and Yih's linear theory and the nonlinear analyses of Benney (1966), Lin (1969), Gjevik (1970) and Nakaya (1975), which involve a long-wave expansion of the velocity field and film height, are more appropriate. Also, if surface tension is small, $We=O(\epsilon)$ or smaller, the curvature term on the right-hand side of (6) can simply be omitted such that surface tension does not enter the problem at all. This often occurs for very large-Reynolds-number flow with thick films. We also note that if $O(\epsilon^2)$ terms are omitted, the lower-order boundary-layer equations of Alekseenko *et al.* (1985) and Bertschy *et al.* (1983) are obtained. Bertschy *et al.* also included higher-order terms in their tangential stress balance. Note, however, that the normal shear term $(2\epsilon/Re)(\partial v/\partial y)$ in (6) is an $O(\epsilon^2)$ term which only appears in this higher-order formulation. This term will give rise to an all-important dissipation term which is necessary for periodic and solitary waves to exist.

Since L is unknown and is merely used in the scaling to correctly appoint the order of each term, we now absorb it by using h_N as the characteristic length for both directions, u_N as the characteristic velocities for both components and h_N/u_N as the characteristic time. The unknown L now disappears from the formulation and ϵ becomes unity in all the equations. This version will be used in subsequent derivations.

The Kármán–Polhausen integral boundary-layer theory involves the following manipulations. Integrating the kinematic equation (5) from $y=0$ to the interface

$y = h$, one obtains from the kinematic equation and continuity equation the mass balance relationship,

$$\frac{\partial h}{\partial t} = -\frac{\partial q}{\partial x}, \tag{11}$$

where

$$q = \int_0^h u \, dy \tag{12}$$

is the local flow rate. Integrating the hydrostatic head of (2) of $y = h$ to y and substituting the value of the liquid pressure at $y = h$ from the normal stress condition (6), an expression for the normal variation of the pressure is obtained. Upon substituting this into the x-momentum equation and again integrating over the film, one obtains the averaged x-momentum equations

$$\frac{\partial q}{\partial t} + \frac{\partial}{\partial x}\left(\frac{\Gamma q^2}{h}\right) = \frac{2}{Re}\int_0^h \frac{\partial}{\partial x}\left(\frac{\partial u}{\partial x}(y = h)\right) dy + We\ (hh_{xxx} - \tfrac{3}{2}hh_x^2 h_{xxx} - 3hh_x h_{xx}^2)$$

$$+ Fr(h\cos\theta - hh_x \sin\theta) + \frac{2}{Re}\int_0^h \frac{\partial^2 u}{\partial x^2} dy - \tau_w + \frac{4}{Re} h_x \frac{\partial u}{\partial x}(y = h), \tag{13}$$

where

$$\Gamma = \frac{h}{q^2}\int_0^h u^2 \, dy \tag{14}$$

is the shape factor (Hanratty 1983) and

$$\tau_w = \frac{1}{Re}\left(\frac{\partial u}{\partial y}\right)(y = 0) \tag{15}$$

is the wall shear. The continuity equation and the tangential stress condition have been used in deriving (13).

A specific profile must now be imposed in this theory. For highly turbulent flow, a flat profile is usually assumed which yields a unity shape factor. However, for the flow of interest, Alekseenko *et al.* have experimentally established that a parabolic profile is more appropriate. Bertschy *et al.* found that this is true even at much higher Reynolds numbers ($Re > 5000$) provided that the waves are far from the entry. Consequently, we impose the following self-similar profile:

$$u = \frac{3q}{h}\left[\left(\frac{y}{h}\right) - \frac{1}{2}\left(\frac{y}{h}\right)^2\right]. \tag{16}$$

It can be easily shown that (16) obeys

$$\frac{\partial u}{\partial x}(y = h) = \frac{\partial}{\partial x}(u(y = h)) = \frac{3}{2}\frac{\partial}{\partial x}\left(\frac{q}{h}\right). \tag{17}$$

The normal velocity v can also be derived from (16) but the only pertinent information is that $\partial v/\partial x$ vanishes at the wall such that the wall shear is simply

$$\tau_w = 3q/Re\, h^2. \tag{18}$$

The parabolic profile also yields a shape factor of 1.2. Introducing these expressions into (13) yields the final averaged x-momentum equation

$$\frac{\partial q}{\partial t} + \frac{\partial}{\partial x}\left(\frac{1.2q^2}{h}\right) = \frac{5}{Re} q_{xx} + We(hh_{xxx} - \tfrac{3}{2}hh_x^2 h_{xxx} - 3hh_x h_{xx}^2)$$

$$+ Fr(h\cos\theta - hh_x \sin\theta) + \frac{3}{Re}\left(\frac{2qh_x^2}{h^2} - \frac{2q_x h_x}{h} - \frac{2qh_{xx}}{h} - \frac{q}{h^2}\right). \tag{19}$$

Two important terms due to the inclusion of the $O(\epsilon^2)$ normal shear term are the dissipation terms $(5/Re)\,q_{xx}$ and $(6/Re)\,qh_{xx}/h$ which do not appear in leading-order boundary-layer theory. If We is $O(\epsilon)$ or smaller, which occurs at high Re, the surface tension terms associated with We in (19) are negligible in the present resolution. This implies that without the dissipation terms, which contains second derivatives of q and h with respect to x, (19) is a nonlinear hyperbolic equation equivalent to the shallow-water equations of Dressler (1949) and Stoker (1957). As Brock (1970) has shown, such a hyperbolic equation does not allow periodic and solitary waveforms. Consequently, we have now explicitly derived the normal shear term empirically introduced by Needham & Merkin (1984) to obtain periodic and solitary waves.

Equations (11) and (19) are then the evolution equations. From the definition of the dimensionless parameters, it can be seen that

$$\frac{3}{Re\,Fr\cos\theta} = 1, \tag{20}$$

which explains the order assignment of (10). Also because of this, an obvious solution to (11) and (19) is the Nusselt flat-film solution

$$\begin{pmatrix} h^* \\ q^* \end{pmatrix} = \begin{pmatrix} 1 \\ 1 \end{pmatrix}. \tag{21}$$

Linearizing (11) and (19) about this base state and taking the partial derivative with respect to t for (11) and with respect to x for (19), one can eliminate the deviation variable for q and obtain a single equation for the deviation film height $\eta = h-1$:

$$\eta_{tt} + 2.4\eta_{xt} + 1.2\eta_{xx} + \frac{3}{Re}[-\tfrac{5}{3}\eta_{txx} + 3\eta_x + \eta_t - \tan\theta\eta_{xx} - 2\eta_{xxx}] + We\eta_{xxxx} = 0. \tag{22}$$

Introducing the normal mode $\eta = \exp[\mathrm{i}(kx-\omega t)]$, where k is the wavenumber and ω the wave frequency, to (22) yields the complex equation

$$-\omega^2 + 2.4k\omega - 1.2k^2 + \frac{3}{Re}[\tfrac{-5}{3}k^2\ \omega\mathrm{i} + 3\mathrm{i}k - \mathrm{i}\omega + \tan\theta k^2 + 2\mathrm{i}k^3] + We\ k^4 = 0. \tag{23}$$

We shall focus only on the temporal instability problem with k real and ω complex. A simple manipulation of (23) yields that the condition for onset, where the first and second derivatives of $\mathrm{Im}\{\omega\}$ with respect to k vanish exactly, is located at

$$Re_c = \tan\theta, \quad \mathrm{Re}\{\omega\}/k = 3, \quad k_c = 0. \tag{24}$$

Since our theory is more appropriate for $Re = O(\epsilon^{-1})$, this prediction of the critical Reynolds number is only acceptable for almost horizontal films, $\tan\theta = O(\epsilon^{-1})$. As expected, the low-Reynolds-number theory of Benjamin (1957) and Yih (1963) yields to leading order $Re_c = \frac{5}{6}\tan\theta$ which is different from (24). We give in the Appendix the approximations invoked in the present theory that causes this deviation from the long-wave expansion for $Re = O(1)$.

In the neighbourhood of the critical Reynolds number where $(Re-\tan\theta) = O(1)$, an expansion of (23) shows that one root is always stable, $\mathrm{Im}\{\omega\} < 0$, while the more unstable one yields

$$\mathrm{Re}\{\omega\} = 3k - 1.2\ Re\ k^3[(Re-\tan\theta) - \tfrac{1}{3}Re\ We\ k^2] + O(\epsilon^4), \tag{25}$$

$$\mathrm{Im}\{\omega\} = (Re-\tan\theta)\,k^2 - \tfrac{1}{3}Re\ We\ k^4 + O(\epsilon^3), \tag{26}$$

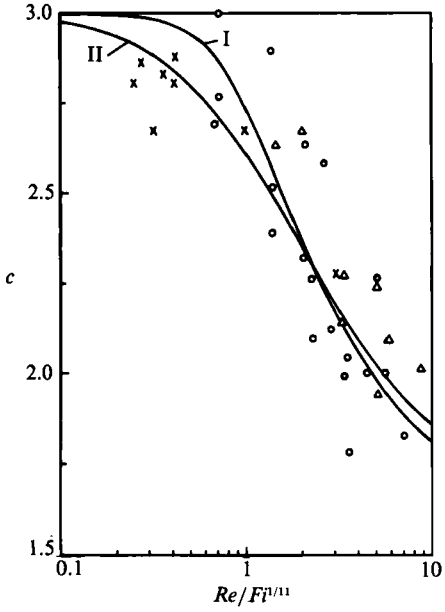

FIGURE 2. comparison of our linear theory to the phase speed of small-amplitude waves near the inlet measured by Alekseenko *et al.* for the vertical film. Curve I corresponds to water with $Fi^{\frac{1}{11}} = 9.54$ and curve II is oil with $Fi^{\frac{1}{11}} = 1.72$. Data for water are marked by crosses and for oil by triangles. The circles denote glycerin–water solution with $Fi^{\frac{1}{11}}$ ranging from 5.42 to 6.78.

where Re is of $O(1)$ and We of $O(\epsilon^{-2})$ in this expansion. A simple manipulation of (26) shows that there are two neutral linear modes with wavenumber zero and

$$k_n = \left[\frac{3(Re - \tan\theta)}{ReWe}\right]^{\frac{1}{2}} \tag{27}$$

and the maximum-growing linear mode is

$$k_m = k_n/\sqrt{2} \tag{28}$$

It is also obvious from (25) and (26) that, near onset, waves with phase velocity $c = \mathrm{Re}\{\omega\}/k$ less than 3 are unstable while the ones travelling faster than thrice the Nusselt velocity are stable. The phase velocity also exhibits a minimum at k_m near onset. These local results break down, however, for conditions far from onset, $Re - Re_c \gg 1$ and numerical solution of (23) must be carried out. In figure 2, we compare the computed phase velocity of the maximum-growing mode of the vertical film against various literature data for infinitesimal waves near inception. The linearized second-order boundary-layer theory, despite the approximation made, seems to adequately describe the phase velocity of these linear waves before they evolve downstream. However, as shown in figure 1, where the dimensional version of the wave frequency $\mathrm{Re}\{\omega\}$ of the maximum-growing mode k_m is compared to the measured frequency of developed waves, the linear theory cannot describe finite-amplitude waves. Finally, we note that for a given fluid with a specified film number Fi, Re and the inclination angle θ completely specify the system since the other parameters in (13), Fr and We, can be derived from (20) and (9), respectively.

3. Weakly nonlinear analysis

Although the integral theory is not the best theory near criticality, $Re = Re_c$, except for nearly horizontal films, we carry out here an analysis near Re_c to demonstrate that solitary waves can only exist with the dissipation term that we have derived from the second-order theory. Moreover, the speed of the solitary waves that we derived near criticality allows us to initiate a numerical continuation scheme to estimate the speed of solitary waves at large Re, away from criticality, which is normally a difficult numerical task. We shall also show that the normal shear terms $(5/Re)\,q_{xx}$ and $(6/Re)\,qh_{xx}/h$ in (19) of our second-order boundary-layer theory allow us to construct all periodic travelling waves near onset ($Re \sim Re_c$). Such waves travel at a dimensionless velocity c without any variation in their shape. Consequently, we transform (11) and (19) into a moving frame by the transformation $x \to x - ct$ and omitting the time dependence in this new coordinate. Integrating the transformed (11) once and using the condition that the Nusselt flat-film base state of (21) must be a solution for all c, one obtains the following relationship between the local flow rate and the film height for the travelling waves:

$$q = 1 + c(h-1). \tag{29}$$

Substituting (29) into the transformed (19) and expanding to second order in the deviation film height η, one obtains

$$\eta_{xxx} = \mu_1\eta + \mu_2\eta_x - \phi\eta_{xx} + \alpha_1\eta^2 + \alpha_2\eta\eta_x + \alpha_3\eta_x^2 + \alpha_4\eta\eta_{xx} + O(|\eta|^3), \tag{30}$$

where
$$\mu_1 = \frac{3}{Re\,We}(c-3), \quad \mu_2 = \frac{1}{We}\left(\frac{3\tan\theta}{Re} - c^2 + 2.4c - 1.2\right),$$

$$\phi = \frac{3}{Re\,We}(\tfrac{5}{3}c - 2),$$

$$\alpha_1 = \frac{9}{Re\,We}(2-c), \quad \alpha_2 = \frac{1}{We}(3.4\,c^2 - 7.2\,c + 3.6),$$

$$\alpha_3 = \frac{6}{Re\,We}(c-1), \quad \alpha_4 = \frac{3}{Re\,We}(\tfrac{11}{3}c - 4).$$

Equation (30) can be rewritten as a dynamical system of three first-order equations

$$\dot{\boldsymbol{u}} = \boldsymbol{L}_0\boldsymbol{u} + \boldsymbol{L}_1\boldsymbol{u} + \begin{pmatrix}0\\0\\1\end{pmatrix} f(\boldsymbol{u}), \tag{31}$$

where $u = (\eta, \eta_x, \eta_{xx})$ and the overdot denotes a derivative with respect to x. The matrices $\boldsymbol{L}_0$ and $\boldsymbol{L}_1$ and the function $f(\boldsymbol{u})$ are

$$\boldsymbol{L}_0 = \begin{pmatrix}0 & 1 & 0\\ 0 & 0 & 1\\ 0 & 0 & -\phi\end{pmatrix}, \quad \boldsymbol{L}_1 = \begin{pmatrix}0 & 0 & 0\\ 0 & 0 & 0\\ \mu_1 & \mu_2 & 0\end{pmatrix},$$

$$f(\boldsymbol{u}) = \alpha_1 u_1^2 + \alpha_2 u_1 u_2 + \alpha_3 u_2^2 + \alpha_4 u_1 u_3.$$

At the critical point of (24), μ_1 and μ_2 vanish exactly and the eigenvalues of the Nusselt fixed point, which has been moved to the origin in (31), are the eigenvalues

of $\boldsymbol{L}_0$, $\{0, 0, -\phi\}$. We shall apply the centre manifold projection and normal form techniques of bifurcation theory to study the dynamics of (31) near the critical point where $\mu_1 = \mu_2 = 0$. In particular, as we have pointed out for other related wave problems (Chang 1987; Hwang & Chang 1987; Chang 1989) we seek periodic orbits (limit cycles) and homoclinic orbits of (31) which correspond to periodic travelling waves and solitary waves. We first note here that the important normal shear term of our second-order boundary-layer theory contributes to the η_{xx} term in (30). The parameter ϕ vanishes exactly for a first-order theory.

Equation (31) is first expanded about $Re_c = \tan\theta$ and $c = 3$. In this expansion, we have isolated the dependence of We on the flow rate by using the identity $We = (3\,Fi/Re^5\cos\theta)^{\frac{1}{3}}$ and stipulating Fi to be a constant for a given fluid. (In our expansion θ and Fi are held constant.) Omitting the detailed similarity transform, near-identity nonlinear transformation, centre manifold expansion and normal form analysis, which we have reported earlier for related problems (Hwang & Chang 1987; Chang 1989), the dynamics of (31) near $\mu_1 = \mu_2 = 0$ is described to leading order by the following Bogdanov–Arnold normal form (Carr 1981), provided that ϕ does not vanish at $\mu_1 = \mu_2 = 0$:

$$\dot{z} = \begin{pmatrix} 0 & 1 \\ 0 & 0 \end{pmatrix} z + \begin{pmatrix} 0 & 0 \\ \nu_1 & \nu_2 \end{pmatrix} z + \begin{pmatrix} 0 \\ -z_1^2 + b z_1 z_2 \end{pmatrix}, \tag{32}$$

where $z \sim u + O(|\mu|\,|u|, |u|^2)$ and the coefficients are

$$\nu_1 = \tfrac{1}{3}(c-3), \quad \nu_2 = -\tfrac{1}{3}(Re - \tan\theta) - \left[\frac{(3Fi/\cos\theta)^{\frac{1}{3}}}{27\,(\tan\theta)^{\frac{2}{3}}} + 0.4\tan\theta\right](c-3),$$

$$b = \tfrac{2}{9}\tan\theta[(3Fi/\cos\theta)^{\frac{1}{3}}/(\tan\theta)^{\frac{5}{3}} + 6.3].$$

The transformation to (32) is only possible if the η_{xx} term in (30) exists. This implies that a first-order boundary-layer theory like those of Dressler and Alekseenko *et al.* would not allow the transformation to (32).

To study the dynamics of (32) for $c < 3$ ($\nu_1 < 0$), we carry out an additional transformation

$$x \to \bar{x}/|\nu_1|^{\frac{1}{2}}, \quad u_1 \to \nu_1(y_1 - 1), \quad u_2 \to |\nu_1|^{\frac{3}{2}} y_2$$

to transfer (32) to

$$\left.\begin{aligned} y_1' &= y_2 + O(\delta^2), \\ y_2' &= y_1 + \sigma y_2 - y_1^2 + \delta y_1 y_2 + O(\delta^2), \end{aligned}\right\} \tag{33}$$

where a prime denotes a derivative with respect to the new spatial coordinate $\bar{x}$ and

$$\delta = -b|\nu_1|^{\frac{1}{2}}, \quad \sigma = \nu_2|\nu_1|^{-\frac{1}{2}} + b|\nu_1|^{\frac{1}{2}}, \tag{34}$$

where δ and σ are small and of order $|\nu_1|^{\frac{1}{2}}$. (The neighbourhood of ν_2 is the same as that for ν_1, $O(\nu_2) \approx O(\nu_1) \ll 1$, and from the scaling we are restricted to small-amplitude waves when $\eta \sim u_1 = O(\nu_1)$.)

At $\sigma = \delta = 0$, which corresponds to a particular path of approaching the double-zero singularity of (24) as specified by (34), (33) becomes conservative and its level curves in the phase plane are given by the first integral

$$H(y_1, y_2) = 3y_1^2 - 2y_1^3 - 3y_2^2 = \beta. \tag{35}$$

These level curves describe a family of limit cycles parameterized by β as shown in figure 3. At $\beta = 1$, one approaches an infinitesimal limit cycle at the fixed point

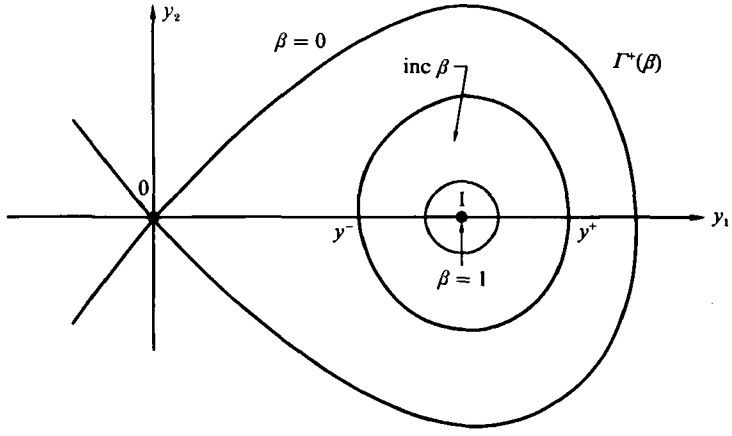

FIGURE 3. Level curves to (33) for $\sigma = \delta = 0$. A homoclinic orbit at $\beta = 0$ encircles a family of periodic orbits parameterized by β from 0 to 1.

$(y_1, y_2) = (1, 0)$ which corresponds to the Nusselt base state of $\eta = \eta_x = 0$. This then provides a closed-form expression for the solitary wave.

A Melnikov analysis allows us to study the dynamics of (33) away from $\sigma = \delta = 0$. In particular, we seek a particular path away from the origin in the (δ, δ)-plane such that a member of the level curves in figure 3 remains intact. This is true for the level curve at parameter β if the Melnikov function $M(\beta)$ vanishes exactly (Guckenheimer & Holmes (1983),

$$M(\beta) = \sigma \int y_2^* \, \mathrm{d}y_1 + \delta \int y_1 y_2^* \, \mathrm{d}y_1 = 0, \tag{36}$$

where the integrals are carried out over the top half of the level curve at β denoted by $y_2^*(y_1; \beta)$ which can be easily obtained from (35). Carr (1981) has analysed the integrals in (36) and discovered that the homoclinic level curve at $\beta = 0$ is invariant along the homoclinic line

$$\sigma = -\tfrac{6}{7}\delta \quad \text{or} \quad \nu_2 = \frac{b}{7}\nu_1$$

or equivalently in the $(Re - \tan\theta)$, $(c-3)$-parameter space

$$Re - \tan\theta = -(5\psi/63 + \tan\theta)\,(c-3), \tag{37}$$

where $\psi = (3Fi/\cos\theta)^{\frac{1}{3}}/(\tan\theta)^{\frac{2}{3}}$. This then provides the speed of the solitary wave near criticality. The Hopf line where the limiting limit cycle at $\beta = 1$ remains invariant lies at

$$\sigma = -\delta \quad \text{or} \quad \nu_2 = 0,$$

which is equivalent to

$$Re - \tan\theta = -\tfrac{1}{3}(\psi + 10.8\tan\theta)\,(c-3). \tag{38}$$

This actually corresponds to the speed of an infinitesimal wave at the neutral wavenumber near criticality, as we shall demonstrate in the next section. In the vertical limit ($\theta \to 0$), both the homoclinic and Hopf lines are tangent to the $(c-3)$-axis. A second-order expansion in $(Re - \tan\theta)$ and $(c-3)$ would be necessary to resolve these lines.

The homoclinic and Hopf lines of (37) and (38) are plotted in the $((Re - Re_c), (c-3))$-parameter space in figure 4 (*a*). Each line within the sector bounded by these two lines

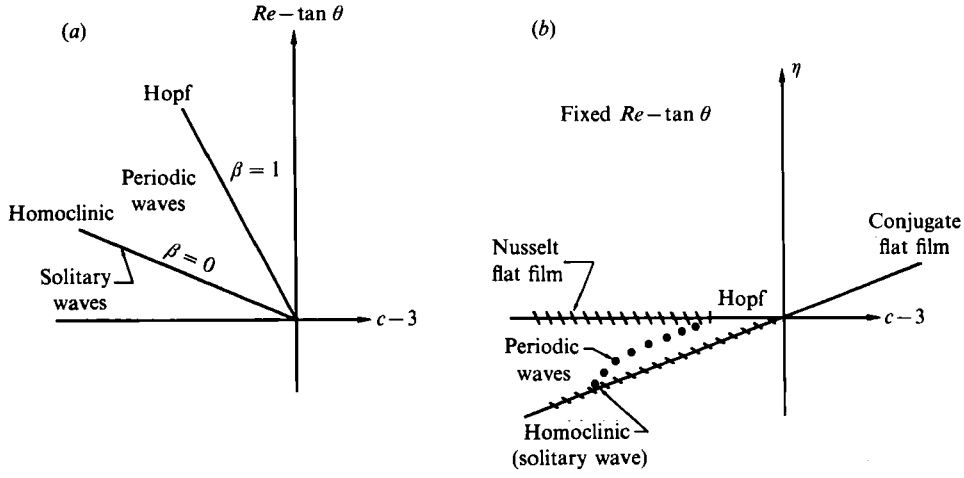

FIGURE 4. The predicted range of periodic and solitary travelling waves near onset and their amplitudes and speeds.

corresponds to a limit cycle with a β-value between zero and one. We have hence established that a family of periodic travelling waves with wavespeed lower than 3 and a solitary travelling wave, which bounds the periodic waves from below in speed, exist for conditions near onset. The 'bifurcation scenario' as c decreases below 3 at a given Re is also schematically depicted in figure 4(*b*). The periodic waves bifurcate supercritically from the Nusselt flat-film base state at the Hopf point and grow in amplitude until they hit the other 'conjugate' flat-film base state for a homoclinic bifurcation. This conjugate flat-film base state, whose thickness varies with c, arises in many travelling wave problems (Benjamin 1984; Chang 1987; Zufiria 1987; Hwang & Chang 1987; Chang 1989). Its thickness, represented by η, is less than that of the Nusselt film for $c < 3$ as represented by the negative η-value. In the present context, it can be easily seen from (19) and (29) that any flat-film solution satisfies

$$(h-1)\,(h^2+h+1-c) = 0, \tag{39}$$

which includes the Nusselt base state $h^* = 1$ as a solution. However, for $c > \frac{3}{4}$, two other flat-film solutions exist. The thicker one bifurcates from the Nusselt base state in a transcritical simple bifurcation at $c = 3$ and is locally given by $\frac{1}{3}(c-3)$, which is that depicted in the local scenario of figure 4(*b*).

The amplitudes and wavelengths of all the periodic waves and the solitary wave can also be estimated from the elliptic integrals associated with the periods along the level curves in figure 3 (Chang 1989). However, such information is of no particular interest here. It should be pointed out, however, that although we have carried out a weakly nonlinear analysis near onset, we have not limited ourselves to a few Fourier harmonics. The Fourier content of the waves shown in figure 3 can be large. Indeed, the solitary wave should have a continuous range of Fourier modes.

4. Strongly nonlinear waves

When Re is much larger than Re_c, the waves evolve rapidly downstream to form large-amplitude waves. Even for small $Re - Re_c$, large-amplitude waves can be generated by artificially paddling the surface or pulsing the liquid feed rate. The fully nonlinear version of (19) and (30) must be analysed to study these large waves.

Carrying out the same manipulations as in the weakly nonlinear analysis but without the Taylor expansion in η, the fully nonlinear dynamical system is now

$$\left.\begin{aligned}
&\dot{u}_1 = u_2, \quad \dot{u}_2 = u_3,\\
&\dot{u}_3 = \Big\{ -cu_2 + \frac{2.4cu_2(1+cu_1)}{1+u_1} - \frac{1.2u_2(1+cu_1)^2}{(1+u_1)^2} - \frac{3}{Re}\Big[\tfrac{5}{3}cu_3 + (1+u_1)\\
&\qquad - u_2\tan\theta(1+u_1) + \frac{2u_2^2(1+cu_1)}{(1+u_1)^2} - \frac{2cu_2^2}{1+u_1} - \frac{2u_3(1+cu_1)}{1+u_1} - \frac{1+cu_1}{(1+u_1)^2}\Big]\Big\}\\
&\qquad \div\{We(1+u_1)(1-\tfrac{3}{2}u_2^2)\} + \frac{3u_3^2u_2}{1-\frac{3}{2}u_2^2}.
\end{aligned}\right\} \quad (40)$$

A particular characteristic of the finite-amplitude travelling shock wave can be immediately deciphered from (40). A shock wave must have vanishing derivatives of η at both upstream and downstream limits. Consequently, η must approach the fixed points of (40) which are simply described by (39). If one specifies that one of the limits must be the Nusselt base state, then the other limit is given by

$$h^2 + h + 1 - c = 0.$$

This equation yields two solutions for $c > \frac{3}{4}$. However, in all our computations, the heteroclinic trajectories of (31), which corresponds to the shocks, connect the Nusselt base state and the thicker solution of this equation for $c < 3$. (For $c > 1$, the thinner solution even yields physically impossible solutions with $h < 0$.) Nevertheless, if one is not concerned with the exact profiles of the shock, the amplitude–velocity relationship of shocks is always given by

$$c - 3 = (h_\infty - 1)^2 + 3(h_\infty - 1),$$

where h_∞ is the film thickness of the shock at the limit that does not correspond to the Nusselt thickness. The quantity $(h_\infty - 1)$ is simply the 'jump' of the shock. Alekseenko *et al.* have also arrived at the same condition for the vertical film from the first-order theory and show that their artificially generated shocks are very well described by this expression.

The periodic and solitary waves, however, must be resolved with a second-order boundary-layer theory. We have carried out a weakly nonlinear analysis for Re near Re_c in the previous section. Away from the critical condition, the leading-order expansion in $Re - Re_c$ and $c - 3$ in the previous section to obtain the Hopf and homoclinic lines is invalid. The Hopf locus must now be determined from the characteristic polynomial of $\boldsymbol{L}_0 + \boldsymbol{L}_1$ in (31),

$$\lambda^3 + \lambda^2\phi - \mu_2\lambda - \mu_1 = 0,$$

which indicates that the Hopf locus is located at

$$\mu_2 = \mu_1\phi, \quad (41)$$

and (38) is a local version of this general result. The homoclinic line and the periodic orbits between the Hopf and homoclinic loci corresponding to the speed at the neutral wavenumber and the solitary wave speed must now be computed numerically. For this purpose, we use a continuation program PEFLOQ (Aluko & Chang 1984) which traces the periodic orbits as a function of c while holding the other parameters constant. It is similar to the AUTO program developed by Doedel & Kernevez (1986). The homoclinic line for the solitary wave speed is also traced by our

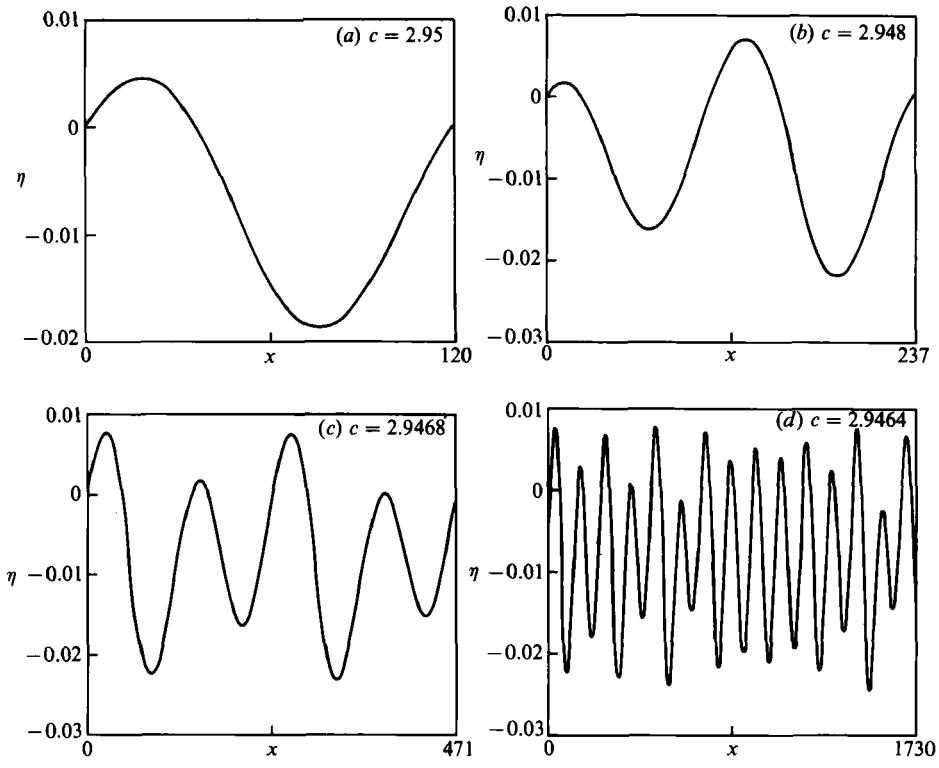

FIGURE 5. Computed wave profiles for $\theta = 80°$ and $Re = 8$ at various wavespeeds near the period-doubling points. The wavelength of each successive wave is hence approximately doubled.

program from the near-critical result of (37). In figure 5, we depict a series of waveforms for water ($Fi^{\frac{1}{11}} = 9.2$) at $\theta = 80°$ and $Re = 8$. In figure 6, we show the computed neutral and solitary wavespeeds for water at $\theta = 0°$, 51° and 80°. The wavespeed measurements of Alekseenko *et al.* and Brauner & Maron (1982) are also shown for comparison. The data seem to indicate that, although a family of periodic travelling waves exists, the film prefers the extremely long ones near the homoclinic line. This explains why the wavelengths of these developed waves cannot be estimated by $2\pi/k_m$ from linear theory, as is shown in figure 1. The reason why waves at higher Re tend to be closer to the solitary wave limit is probably because the linear growth rate at low Re is too low to allow the final solitary waves to evolve within the length of the laboratory channels. This also explains why the vertical film seems to reach the solitary wave limit at a lower Re.

The computed homoclinic locus converges with the Hopf locus at large Re. This is not surprising since when Re approaches infinity (or $O(\epsilon^{-2})$ in the present formulation), the Weber number We approaches zero for a given fluid, and the normal stress term also vanishes such that (19) reduces to a first-order differential equation in the moving coordinate and does not permit any periodic wave solution between the Hopf and homoclinic loci. This singular limit is also evident in (30) and (31). From (41), this limit occurs at the wave velocity

$$c_{1\mathrm{lm}} = 1.69 \tag{42}$$

which the neutral wave velocity at large Re. Consequently, the solitary waves and periodic waves all approach a limiting velocity at large Re that is 1.69 times the

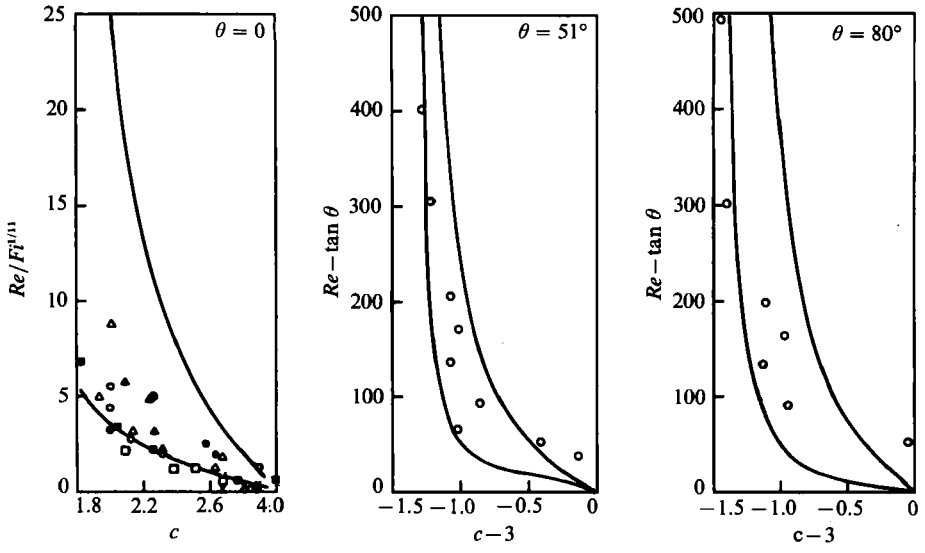

FIGURE 6. Comparison of experimental data of Alekseenko *et al.* ($\theta = 0°$) and Brauner & Maron ($\theta = 51°$ and $80°$) to the computed Hopf (upper) and homoclinic (lower) curves. While the data generally lie between the two curves, a shift towards the homoclinic limit is seen at higher Reynolds numbers. ○, △, aqueous glycerin; ●, aqueous glycerin–ethanol; ▲, aqueous ethanol; □, water. These data span a large range of viscosity and surface tension.

Nusselt velocity. Another quantitative estimate can be made at this high-Re limit. Since all solitary waves approach the conjugate flat film both upstream and downstream, we can estimate the substrate thickness of the high-Re solitary waves from (39), which is valid for all c and Re. Substituting (42) into (39), one obtains

$$h_s = 0.47 \tag{43}$$

or that the substrates are 0.47 as thick as the Nusselt film thickness. No information about the amplitude of the wave peak can be obtained. We have already seen in figure 6 that (42) is in agreement with the high-Re data of Alekseenko *et al.* and Brauner & Maron (1982). In figure 7, dimensional versions of (42) and (43) are compared to the vertical-film data of Chu & Dukler (1974, 1975) for water, which were organized by Brauner & Maron (1983). It is interesting to note that average film thickness at high Re is often found to be significantly lower than the Nusselt thickness h_N (Brauner 1987). If the surface is indeed covered by the solitary waves, the substrate will occupy a larger portion of the film than the peaks, which are in excess of h_N, and a small average film thickness will result. Finally, we note that if a flat velocity profile was imposed instead of (16), the shape factor Γ of (14) becomes unity and the limiting velocity at high Reynolds number of (42) is now 1.5. This is precisely the limiting velocity found by Hwang & Chang (1987) for Dressler's shallow-water equation with the empirical dissipation term of Needham & Merkin (1984) for turbulent inclined flow.

5. Period-doubling evolution towards long waves

In the last two sections, we have constructed a family of periodic waveforms and a solitary waveform for any given condition. However, their stability has not been determined. In fact, the measurements of Alekseenko *et al.* and Brauner & Maron

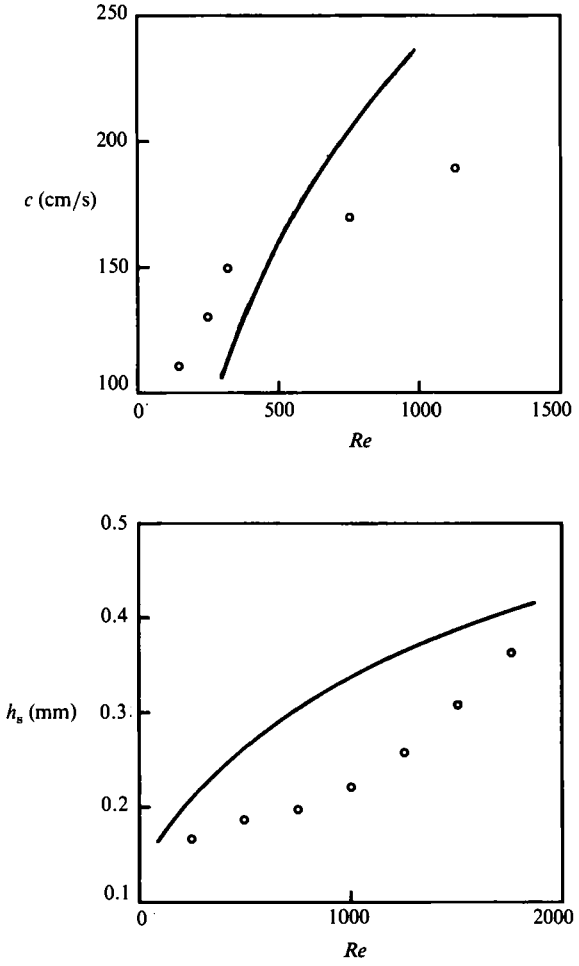

FIGURE 7. Comparison of wavespeed and substrate thickness measured by Chu & Dukler for well-developed vertical waves to our predictions of (42) and (43) from the solitary wave limit. $\theta = 0$.

(1982) suggest that all periodic waves are unstable to subharmonic instability and this successive period-doubling selection process eventually yields the solitary waveform, which is the preferred waveform, downstream. We confirm this observation here by showing that short monochromatic waves near the neutral curve are unstable to subharmonic disturbances. Our amplitude equation approach is similar to that of Janssen (1986) for period doubling of sheared gravity–capillary waves. However, we derive the amplitude equations, which are valid to third order here instead of his second-order equations, via the centre-manifold projection technique of Carr (1981).

We shall carry out our subharmonic stability analysis near the neutral curve, which can be far from criticality such that $Re = O(\epsilon^{-1})$ as stipulated by our derivation of (11) and (19). We begin by reinserting the perturbation parameter ϵ to identify the order of each term in (19). This is done by the following transformation which reflects the correct order of each variable and parameter:

$$Re \to Re\ \epsilon^{-1}, \quad We \to We\ \epsilon^{-2}, \quad Fr \to Fr\ \epsilon, \quad x \to x\ \epsilon^{-1}, \quad t \to t\,\epsilon^{-1}.$$

The deviation film height and flow rate, η and ξ, are defined as

$$\eta = h-1, \quad \xi = q-1, \tag{44a, b}$$

and are stipulated to be of $O(\epsilon)$. Expanding (19) in η and ξ and collecting terms up to $O(\epsilon^2)$, the resulting equations, after reabsorbing ϵ as before, are

$$\eta_t = -\xi_x, \tag{45a}$$

$$\begin{aligned}\xi_t = &-2.4\xi_x + 1.2\eta_x + We\,\eta_{xxx} + \frac{9}{Re}\eta - \frac{3}{Re}\xi - \frac{3}{\mathrm{Re}}\tan\theta\eta_x + \frac{5}{Re}\xi_{xx} - \frac{6}{Re}\eta_{xx} \\ &-2.4\xi\xi_x + 2.4\eta\xi_x + 2.4\xi\eta_x - \left(2.4 + \frac{3}{Re}\tan\theta\right)\eta\eta_x - \frac{9}{Re}\eta^2 + \frac{6}{Re}\eta\xi + We\,\eta\eta_{xxx} \\ &+\frac{12}{Re}\eta^3 - \frac{9}{Re}\xi\eta^2 - 4.8\xi\eta\eta_x + 2.4\eta\xi\xi_x - 2.4\eta^2\xi_x + 1.2\xi^2\eta_x + 3.6\eta^2\eta_x,\end{aligned} \tag{45b}$$

which can be written as

$$\boldsymbol{u}_t = \boldsymbol{L}\boldsymbol{u} + \boldsymbol{N}(\boldsymbol{u}) \tag{46}$$

where $\boldsymbol{u} = (\eta, \xi)^{\mathrm{T}}$ and the linear stability of the Nusselt flat-film basic state is determined by the eigenvalue problem

$$\boldsymbol{L}\boldsymbol{w}_l = \lambda \boldsymbol{w}_l \quad (l = 1, 2) \tag{47a}$$

where

$$\boldsymbol{L} = \begin{pmatrix} 0 & -\dfrac{\partial}{\partial x} \\ a_0 + a_1\dfrac{\partial}{\partial x} + a_2\dfrac{\partial^2}{\partial x^2} + a_3\dfrac{\partial^3}{\partial x^3} & b_0 + b_1\dfrac{\partial}{\partial x} + b_2\dfrac{\partial^2}{\partial x^2} \end{pmatrix} \tag{47b}$$

$$\left.\begin{aligned} a_0 = \frac{9}{Re}, \quad a_1 = 1.2 - 3\tan\theta/Re, \quad a_2 = -6/Re, \quad a_3 = We; \\ b_0 = -3/Re, \quad b_1 = -2.4, \quad b_2 = 5/Re. \end{aligned}\right\} \tag{47c}$$

Since the coefficients of $\boldsymbol{L}$ are independent of x, one can Fourier transform (47a) in x, which is equivalent to the following normal mode substitution:

$$\boldsymbol{w}_l(x) = \boldsymbol{v}_l \exp(\mathrm{i}kx). \tag{48}$$

After inserting (48) into (47a), one obtains the equivalent eigenvalue problem

$$\boldsymbol{A}(k)\,\boldsymbol{v}_l = \lambda_l(k)\,\boldsymbol{v}_l \quad (l = 1, 2), \tag{49}$$

where

$$\boldsymbol{A}(k) = \begin{pmatrix} 0 & \mathrm{i}k \\ \alpha_{\mathrm{r}} + \mathrm{i}\alpha_{\mathrm{i}} & \beta_{\mathrm{r}} + \mathrm{i}\beta_{\mathrm{i}} \end{pmatrix}, \tag{50}$$

$$\begin{aligned} \alpha_{\mathrm{r}}(k) = a_0 - a_2 k^2, \quad \alpha_{\mathrm{i}}(k) = a_1 k - a_3 k^3 \\ \beta_{\mathrm{r}}(k) = b_0 - b_2 k^2, \quad \beta_{\mathrm{i}}(k) = b_1 k. \end{aligned}$$

The eigenvalues of the complex $\boldsymbol{A}$ are then simply

$$\lambda_1(k) = \tfrac{1}{2}[\beta_{\mathrm{r}} + \mathrm{i}\beta_{\mathrm{i}} - \gamma(k)], \quad \lambda_2(k) = \tfrac{1}{2}[\beta_{\mathrm{r}} + \mathrm{i}\beta_{\mathrm{i}} + \gamma(k)], \tag{51a, b}$$

where the complex number γ is

$$\gamma(k) = [-4k(\mathrm{i}\alpha_{\mathrm{r}} - \alpha_{\mathrm{i}}) + (\beta_{\mathrm{r}} + \mathrm{i}\beta_{\mathrm{i}})^2]^{\frac{1}{2}} \tag{51c}$$

and the eigenvectors are

$$v_1(k) = d_1\begin{pmatrix} -\mathrm{i}k/\lambda_1(k) \\ 1 \end{pmatrix}, \quad v_2(k) = d_2\begin{pmatrix} -\mathrm{i}k/\lambda_2(k) \\ 1 \end{pmatrix}, \tag{51d, e}$$

where the normalizing constants $d_l(k)$ are

$$d_l(k) = \lambda_l^2/[\lambda_l^2 - \mathrm{i}k(\alpha_r + \mathrm{i}\alpha_i)]. \tag{50f}$$

We note that $\lambda_2(k)$ is always stable and $\lambda_1(k)$ is the eigenvalue that destabilizes at the neutral curve.

The adjoint eigenvalue problem to (49) is

$$\boldsymbol{A}^{\mathrm{T}}(k)\,\hat{\boldsymbol{v}}_l(k) = \lambda_l(k)\,\hat{\boldsymbol{v}}_l(k) \quad (l = 1, 2) \tag{52}$$

such that

$$\hat{\boldsymbol{v}}_l = \begin{pmatrix} (\alpha_r + \mathrm{i}\alpha_i)/\lambda_l(k) \\ 1 \end{pmatrix} \quad (l = 1, 2) \tag{53}$$

and the orthogonality condition holds:

$$\hat{\boldsymbol{v}}_l(k) \cdot \hat{\boldsymbol{v}}_m(k) = \delta_{lm}. \tag{54}$$

We can now expand $\boldsymbol{u}$ of(46) in terms of the eigenvectors $\boldsymbol{v}_l$,

$$\boldsymbol{u} = \sum_{l,m} a_{l,m}(t)\,\boldsymbol{v}_l(m\tfrac{1}{2}k_0)\exp(\mathrm{i}m\tfrac{1}{2}k_0 x) + \text{complex conjugate}, \tag{55}$$

where we have imposed a periodicity of $4\pi k_0$ such that the fundamental k_0 corresponds to $m = 2$ and the subharmonic $\frac{1}{2}k_0$ to $m = 1$. The wavenumber k_0 is yet unspecified. Substituting (55) into (45) and taking the inner product with $\hat{\boldsymbol{v}}_l\,(\frac{1}{2}mk_0)\exp(-\frac{1}{2}\mathrm{i}mk_0 x)$, one obtains the amplitude equations for $1 < m < 4$:

$$\frac{\mathrm{d}a_{11}}{\mathrm{d}t} = \lambda_1(\tfrac{1}{2}k_0)\,a_{11} + P_{11}\,a_{12}\,a_{11}^* + P_{21}\,a_{22}\,a_{11}^* + P_{31}\,a_{12}\,a_{21}^* + P_{41}\,a_{13}\,a_{12}^* + P_{51}\,a_{23}\,a_{12}^* + P_{61}\,a_{11}^2\,a_{11}^* + P_{71}\,a_{11}\,a_{12}\,a_{12}^* + O(4), \tag{56a}$$

$$\frac{\mathrm{d}a_{21}}{\mathrm{d}t} = \lambda_2(\tfrac{1}{2}k_0)\;a_{21} + Q_{11}\,a_{12}\,a_{11}^* + O(3), \tag{56b}$$

$$\frac{\mathrm{d}a_{12}}{\mathrm{d}t} = \lambda_1(k_0)\,a_{12} + P_{12}\,a_{11}^2 + P_{22}\,a_{11}\,a_{21} + P_{32}\,a_{11}^*\,a_{13} + P_{42}\,a_{11}^*\,a_{23} + P_{52}\,a_{12}^*\,a_{14} + P_{62}\,a_{12}^*\,a_{24} + P_{72}\,a_{11}\,a_{12}\,a_{11}^* + P_{82}\,a_{12}^*\,a_{12}^2 + O(4), \tag{56c}$$

$$\frac{\mathrm{d}a_{22}}{\mathrm{d}t} = \lambda_2(k_0)\,a_{22} + Q_{12}\,a_{11}^2 + O(3), \tag{56d}$$

$$\frac{\mathrm{d}a_{13}}{\mathrm{d}t} = \lambda_2(\tfrac{3}{2}k_0)\,a_{13} + P_{13}\,a_{11}\,a_{12} + O(3), \tag{56e}$$

$$\frac{\mathrm{d}a_{23}}{\mathrm{d}t} = \lambda_2(\tfrac{3}{2}k_0)\,a_{23} + Q_{13}\,a_{11}\,a_{12} + O(3), \tag{56f}$$

$$\frac{\mathrm{d}a_{14}}{\mathrm{d}t} = \lambda_1(2k_0)\,a_{14} + P_{14}\,a_{12}^2 + O(3), \tag{56g}$$

$$\frac{\mathrm{d}a_{24}}{\mathrm{d}t} = \lambda_2(2k_0)\,a_{24} + Q_{14}\,a_{12}^2 + O(3), \tag{56h}$$

where superscript * denotes complex conjugate. If the nonlinearity $\boldsymbol{N}(\boldsymbol{u})$ of (46) is expanded to quadratic and cubic terms,

$$\boldsymbol{D}(\boldsymbol{u}_1, \boldsymbol{u}_2) = \frac{1}{2}\frac{\partial^2}{\partial\delta_1\,\partial\delta_2}\boldsymbol{N}(\delta_1\boldsymbol{u}_1+\delta_2\boldsymbol{u}_2)\Big|_{\delta_1=\delta_2=0}, \tag{57a}$$

$$\boldsymbol{T}(\boldsymbol{u}_1, \boldsymbol{u}_2, \boldsymbol{u}_3) = \frac{1}{3!}\frac{\partial^3}{\partial\delta_1\,\partial\delta_2\,\partial\delta_3}\boldsymbol{N}(\delta_1\boldsymbol{u}_1+\delta_2\boldsymbol{u}_2+\delta_3\boldsymbol{u}_2)\Big|_{\delta_1=\delta_2=\delta_3=0} \tag{57b}$$

then the nonlinear interaction coefficients P_{ij} and Q_{ij} can be expressed formally as

$$P_{ml} = P'_{ml}\,\hat{v}_1(l\tfrac{1}{2}k_0)\exp(-\mathrm{i}l\tfrac{1}{2}k_0 x), \tag{58a}$$

$$Q_{ml} = P'_{ml}\,\hat{v}_2(l\tfrac{1}{2}k_0)\exp(-\mathrm{i}l\tfrac{1}{2}k_0 x), \tag{58b}$$

where for $j = 1, 2$

$$P'_{j1} = 2\boldsymbol{D}(\boldsymbol{v}_1^*(\tfrac{1}{2}k_0)\exp(-\mathrm{i}\tfrac{1}{2}k_0 x), \boldsymbol{v}_j(k_0)\exp(\mathrm{i}k_0 x)), \tag{58c}$$

$$P'_{31} = 2\boldsymbol{D}(\boldsymbol{v}_2^*(\tfrac{1}{2}k_0)\exp(-\mathrm{i}\tfrac{1}{2}k_0 x), \boldsymbol{v}_1(k_0)\exp(\mathrm{i}k_0 x)), \tag{58d}$$

$$P'_{j+3,1} = 2\boldsymbol{D}(\boldsymbol{v}_1^*(k_0)\exp(-\mathrm{i}k_0 x), \boldsymbol{v}_j(\tfrac{3}{2}k_0)\exp(3\mathrm{i}\tfrac{1}{2}k_0)), \tag{58e}$$

$$P'_{j+5,1} = 3\boldsymbol{T}(\boldsymbol{v}_1(\tfrac{1}{2}k_0)\exp(\mathrm{i}\tfrac{1}{2}k_0 x), \boldsymbol{v}_1(j\tfrac{1}{2}k_0)\exp(\mathrm{i}j\tfrac{1}{2}k_0\,x), \boldsymbol{v}_1^*(j\tfrac{1}{2}k_0)\exp(-\mathrm{i}j\tfrac{1}{2}k_0\,x))j \tag{58f}$$

$$P'_{j,2} = \boldsymbol{D}(\boldsymbol{v}_1(\tfrac{1}{2}k_0)\exp(\mathrm{i}\tfrac{1}{2}k_0\,x), \boldsymbol{v}_j(\tfrac{1}{2}k_0)\exp(\mathrm{i}\tfrac{1}{2}k_0 x)), \tag{58g}$$

$$P'_{j+2,2} = 2\boldsymbol{D}(\boldsymbol{v}_1^*\,(\tfrac{1}{2}k_0)\exp(-\mathrm{i}\tfrac{1}{2}k_0 x), \boldsymbol{v}_j(\tfrac{3}{2}k_0)\exp(\mathrm{i}\tfrac{3}{2}k_0\,x), \tag{57h}$$

$$P'_{j+4,2} = 2\boldsymbol{D}(\boldsymbol{v}_1^*(k_0)\exp(-\mathrm{i}\tfrac{1}{2}k_0 x), \boldsymbol{v}_j(2k_0)\exp(\mathrm{i}2k_0 x)), \tag{58i}$$

$$P'_{j+6,2} = 6\boldsymbol{T}(\boldsymbol{v}_1(k_0)\exp(\mathrm{i}k_0 x), \boldsymbol{v}_1(j\tfrac{1}{2}k_0)\exp(\mathrm{i}j\tfrac{1}{2}k_0 x), \boldsymbol{v}_1^*(j\tfrac{1}{2}k_0)\exp(-\mathrm{i}j\tfrac{1}{2}k_0 x))j. \tag{58j}$$

If k_0 is the neutral wavenumber k_n,

$$\lambda_1^{\mathrm{r}}(k_n) = 0, \tag{59a}$$

where the superscript r denotes the real part, then because all wavenumbers larger than k_n are stable and all wavenumbers smaller than k_n are unstable

$$\lambda_1^{\mathrm{r}}(\tfrac{1}{2}k_n) > 0, \quad \lambda_2^{\mathrm{r}}(\tfrac{1}{2}k_n) < 0, \quad \lambda_l^{\mathrm{r}}(m\tfrac{1}{2}k_n) < 0 \quad (l = 1, 2, \quad m \geqslant 3). \tag{59b}$$

Then by the centre-manifold projection theorem (Carr 1981; Guckenheimer & Holmes 1983) and the related unstable-centre-manifold theorem (Armbruster, Guckenheimer & Holmes 1988), the stable modes can be expanded in terms of the neutral mode a_{12} and the unstable mode a_{11} such that the dynamics of (56) can be approximated by two amplitude equations. To leading non-vanishing order, these stable modes are second order in the neutral and unstable modes. Consequently, second-order resolution suffices in the amplitude equations of the stable modes in (56). The centre-manifold expansion is then, from (56),

$$a_{21} \sim -\frac{Q_{11}\,a_1\,a_{\frac{1}{2}}^*}{\lambda_2(\frac{1}{2}k_n)-\lambda_1^*(\frac{1}{2}k_n)-\mathrm{i}\omega}, \quad a_{22} \sim -\frac{Q_{12}\,a_{\frac{1}{2}}^2}{\lambda_2(k_n)-2\lambda_1(\frac{1}{2}k_n)}, \tag{60a, b}$$

$$a_{13} \sim -\frac{P_{13}\,a_{\frac{1}{2}}\,a_1}{\lambda_1(\frac{3}{2}k_n)-\lambda_1(\frac{1}{2}k_n)-\mathrm{i}\omega}, \quad a_{23} \sim -\frac{Q_{13}\,a_{\frac{1}{2}}\,a_1}{\lambda_2(\frac{3}{2}k_n)-\lambda_1(\frac{1}{2}k_n)-\mathrm{i}\omega}, \tag{60c, d}$$

$$a_{14} \sim -\frac{P_{14}\,a_1^2}{\lambda_1(2k_n)-2\mathrm{i}\omega}, \quad a_{24} \sim -\frac{Q_{14}\,a_1^2}{\lambda_2(2k_n)-2\mathrm{i}\omega}, \tag{60e, f}$$

where the frequency $\mathrm{i}\omega$ is simply $\lambda_1(k_n)$ which is purely imaginary by (59a), and we

have also simplified the notation for the fundamental and subharmonic modes such that $a_1 = a_{12}$ and $a_{\frac{1}{2}} = a_{11}$. Substituting (60) into (56a) and (56c), we then obtain the projected amplitude equations

$$\frac{\mathrm{d}a_{\frac{1}{2}}}{\mathrm{d}t} = \lambda_1(\tfrac{1}{2}k_\mathrm{n})\,a_{\frac{1}{2}} + C_1\,a_1\,a_{\frac{1}{2}}^* + C_2\,a_{\frac{1}{2}}^*\,a_{\frac{1}{2}}^2 + C_3\,|a_1|^2\,a_{\frac{1}{2}}, \tag{61a}$$

$$\frac{\mathrm{d}a_1}{\mathrm{d}t} = \mathrm{i}\omega a_1 + D_1\,a_{\frac{1}{2}}^2 + D_2\,a_1^*\,a_1^2 + D_3\,|a_{\frac{1}{2}}|^2\,a_1, \tag{61b}$$

which is valid to $O(3)$ in $|a_{\frac{1}{2}}|$ and $|a_1|$. The complex coefficients are

$$C_1 = P_{11}, \quad C_2 = P_{61} - \frac{P_{21}\,Q_{12}}{\lambda_2(k_\mathrm{n}) - 2\lambda_1(\frac{1}{2}k_\mathrm{n})}, \tag{62a, b}$$

$$C_3 = P_{71} - \frac{P_{51}\,Q_{13}}{\lambda_2(\frac{3}{2}k_\mathrm{n}) - \lambda_1(\frac{1}{2}k_\mathrm{n}) - \mathrm{i}\omega} - \frac{P_{41}\,P_{13}}{\lambda_1(\frac{3}{2}k_\mathrm{n}) - \lambda_1(\frac{1}{2}k_\mathrm{n}) - \mathrm{i}\omega} - \frac{P_{31}\,Q_{11}^*}{\lambda_2^*(\frac{1}{2}k_\mathrm{n}) - \lambda_1(\frac{1}{2}k_\mathrm{n}) + \mathrm{i}\omega}, \tag{62c}$$

$$D_1 = P_{12}, \quad D_2 = P_{82} - \frac{P_{62}\,Q_{14}}{\lambda_2(2k_\mathrm{n}) - 2\mathrm{i}\omega} - \frac{P_{52}\,P_{14}}{\lambda_1(2k_\mathrm{n}) - 2\mathrm{i}\omega}, \tag{62d, e}$$

$$D_3 = P_{72} - \frac{P_{32}\,P_{13}}{\lambda_1(\frac{3}{2}k_\mathrm{n}) - \lambda_1(\frac{1}{2}k_\mathrm{n}) - \mathrm{i}\omega} - \frac{P_{42}\,Q_{13}}{\lambda_2(\frac{3}{2}k_\mathrm{n}) - \lambda_1(\frac{1}{2}k_\mathrm{n}) - \mathrm{i}\omega} - \frac{P_{22}\,Q_{11}}{\lambda_2(\frac{1}{2}k_\mathrm{n}) - \lambda_1^*(\frac{1}{2}k_\mathrm{n}) - \mathrm{i}\omega}. \tag{62f}$$

If k_0 is slightly lower than the neutral wavenumber k_n such that $k_0 - k_\mathrm{n}$ is $O(2)$ in $|a_{\frac{1}{2}}|$ and $|a_1|$, the linear terms in (61) need to be expanded to leading order in $k_0 - k_\mathrm{n}$ to yield

$$\frac{\mathrm{d}a_{\frac{1}{2}}}{\mathrm{d}t} = (\lambda_1(\tfrac{1}{2}k_\mathrm{n}) + \sigma_{\frac{1}{2}})\,a_{\frac{1}{2}} + C_1\,a_1\,a_{\frac{1}{2}}^* + C_2\,|a_{\frac{1}{2}}|^2\,a_{\frac{1}{2}} + C_3\,|a_1|^2\,a_{\frac{1}{2}}, \tag{63a}$$

$$\frac{\mathrm{d}a_1}{\mathrm{d}t} = (\mathrm{i}\omega + \sigma_1)\,a_1 + D_1\,a_{\frac{1}{2}}^2 + D_2\,|a_1|^2\,a_1 + D_3\,|a_{\frac{1}{2}}|^2\,a_1, \tag{63b}$$

where the complex perturbations to the eigenvalues are

$$\sigma_{\frac{1}{2}} = \left(\frac{\partial\lambda_1}{\partial k}\right)(\tfrac{1}{2}k_\mathrm{n})^{\frac{1}{2}}\,(k_0 - k_\mathrm{n}), \quad \sigma_1 = \left(\frac{\partial\lambda_1}{\partial k}\right)(k_\mathrm{n})\,(k_0 - k_\mathrm{n}). \tag{64a, b}$$

We are hence perturbing from k_n such that k_0 lies in a small neighbourhood below k_n and $a_{\frac{1}{2}}$ and a_1 are resolved to $O(|k_0 - k_\mathrm{n}|^{0.5})$ by (63).

Equation (63) can be further simplified by the following moving coordinate transformation:

$$a_{\frac{1}{2}} \to a_{\frac{1}{2}} \exp(-\tfrac{1}{2}\mathrm{i}\hat{\omega}t), \quad a_1 \to a_1 \exp(-\mathrm{i}\hat{\omega}t), \tag{65a, b}$$

where the wave frequency is

$$\hat{\omega} = -\omega - \sigma_1^\mathrm{i} + D_2^\mathrm{i}\,\sigma_1^\mathrm{r}/D_2^\mathrm{r}, \tag{65c}$$

the superscripts r and i denoting real and imaginary parts, respectively. Equation (63) then reduces to

$$\frac{\mathrm{d}a_{\frac{1}{2}}}{\mathrm{d}t} = [\lambda_1(\tfrac{1}{2}k_\mathrm{n}) + \sigma_{\frac{1}{2}} + \tfrac{1}{2}\hat{\omega}\mathrm{i}]\,a_{\frac{1}{2}} + C_1\,a_1\,a_{\frac{1}{2}}^* + C_2\,|a_{\frac{1}{2}}|^2\,a_{\frac{1}{2}} + C_3\,|a_1|^2\,a_{\frac{1}{2}}, \tag{66a}$$

$$\frac{\mathrm{d}a_1}{\mathrm{d}t} = \sigma_1^\mathrm{r}(1 + iD_2^\mathrm{i}/D_2^\mathrm{r})\,a_1 + D_1\,a_{\frac{1}{2}}^2 + D_2\,|a_1|^2\,a_1 + D_3\,|a_{\frac{1}{2}}|^2\,a_1. \tag{66b}$$

If the subharmonic amplitude is set to zero in (66), the resulting amplitude equation for the fundamental

$$\frac{\mathrm{d}a_1}{\mathrm{d}t} = \sigma_1^{\mathrm{r}}(1+\mathrm{i}D_2^{\mathrm{i}}/D_2^{\mathrm{r}})\,a_1 + D_2|a_1|^2\,a_1 \tag{67}$$

is simply the classical Stuart–Landau equation and it determines the bifurcation of monochromatic waves near the neutral curve. This is essentially the same Hopf bifurcation off the neutral curve (Hopf line) in figure 4 although we use the wavenumber k as the bifurcation parameters here instead of the wavevelocity c. It is clear from (64) that this finite-amplitude monochromatic wave which bifurcates supercritically at the neutral curve k_{n} has an amplitude of

$$|a_1| = (-\sigma_1^{\mathrm{r}}/D_2^{\mathrm{r}})^{\frac{1}{2}}. \tag{68}$$

Linearizing (67) about (68), one obtains the eigenvalue $-\sigma_1^{\mathrm{r}}$ which implies that all supercritical finite-amplitude monochromatic waves are stable to disturbances of the same wavelength.

Stability of the monochromatic wave to subharmonic disturbances is, however, quite different. To study this subharmonic instability we linearize (66) about (68) and $a_{\frac{1}{2}} = 0$. The resulting Jacobians for the subharmonic conjugate pairs are decoupled from the Jacobian for the fundamental, which yields the same stable eigenvalue $-\sigma_1^{\mathrm{r}}$ for disturbances with the fundamental wavenumber as before. The Jacobian for the subharmonic disturbances is

$$\boldsymbol{J} = \begin{pmatrix} J_1 & J_2 \\ J_2^* & J_1^* \end{pmatrix}, \tag{69a}$$

where

$$J_1 = \lambda_1(\tfrac{1}{2}k_{\mathrm{n}}) + \sigma_{\frac{1}{2}} + \tfrac{1}{2}\mathrm{i}\hat{\omega} - C_3\,\sigma_1^{\mathrm{r}}/D_2^{\mathrm{r}}, \tag{69b}$$

$$J_2 = C_1\,a_1, \tag{69c}$$

such that the trace and determinant of $\boldsymbol{J}$ are

$$\text{trace} = J_1 + J_1^* = \lambda_1^{\mathrm{r}}(\tfrac{1}{2}k_{\mathrm{n}}) + \sigma_{\frac{1}{2}}^{\mathrm{r}} - C_3^{\mathrm{r}}\,\sigma_1^{\mathrm{r}}/D_2^{\mathrm{r}}, \tag{70a}$$

$$\det = |J_1|^2 - |J_2|^2 = |J_1|^2 - |C_1|^2\,|a_1|^2. \tag{70b}$$

The necessary and sufficient condition for the waveforms near the neutral curve to be stable to subharmonic disturbances is then

$$\text{trace} < 0, \tag{71a}$$

$$\det > 0. \tag{71b}$$

For all inclination angles and Re, which completely specify the system, we find the determinant condition to be satisfied near the neutral curve. Consequently, only the trace condition is pertinent. From (70a) and the definition of σ_i in (64), it is clear that the trace condition is a local approximation of

$$\lambda_1^{\mathrm{r}}(\tfrac{1}{2}k_0) < (C_3^{\mathrm{r}}/D_2^{\mathrm{r}})\,\lambda_1^{\mathrm{r}}(k_0), \tag{72}$$

where k_0 is a wavenumber slightly lower than the neutral one k_{n}. By definition, the fundamental and its subharmonic are unstable, $\lambda_1^{\mathrm{r}}(k_0) > 0$ and $\lambda_1^{\mathrm{r}}(\frac{1}{2}k_0) > 0$. Consequently, a sufficient condition for all monochromatic waves to be unstable is $(C_3^{\mathrm{r}}/D_2^{\mathrm{r}}) < 0$. This is not the case, however, for the present system. For positive $(C_3^{\mathrm{r}}/D_2^{\mathrm{r}})$, wavenumbers very near k_{n} should be unstable since the right-hand side of (72) is small. However, as k_0 departs sufficiently from k_{n}, the growth rate of the

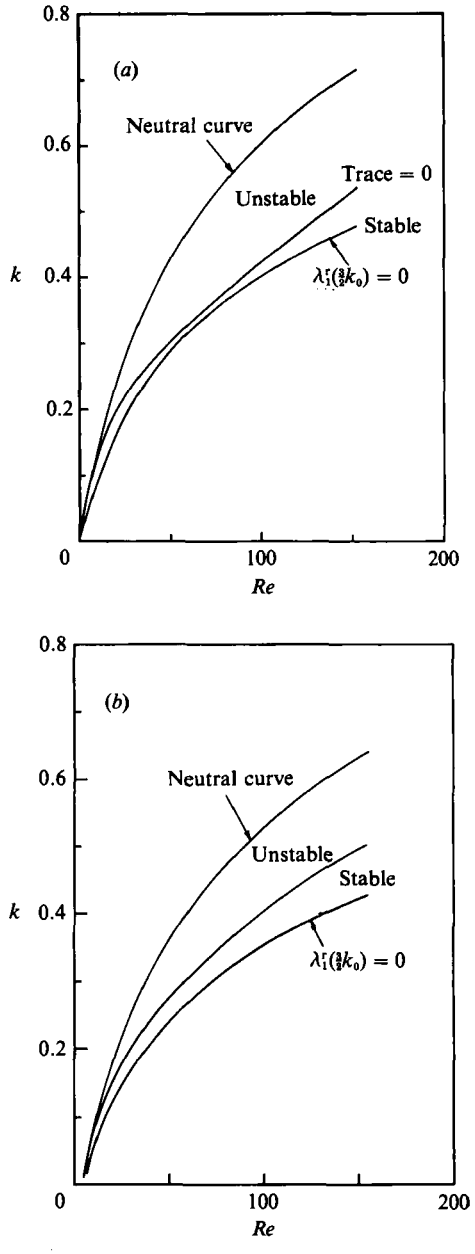

FIGURE 8. The band of monochromatic waves unstable to subharmonic instability for water at an inclination angle of (*a*) 51°, (*b*) 80°. The neutral curve of the $\frac{3}{2}$ mode is also shown.

fundamental becomes sufficiently large compared to its subharmonic and (72) is satisfied. Consequently, there exists a band of periodic waves near the neutral curve, whose bandwidth is inversely related to the parameter (C_3^r/D_2^r), that are unstable to subharmonic instability. In figure 8 we have depicted the computed curve for trace $= 0$ from (68*a*). Also depicted is the neutral curve for the $\frac{3}{2}$ mode, $\lambda_1^r(\frac{3}{2}k_0) = 0$. Since our analysis assumed that we are sufficiently close to the neutral curve that all modes except the k_0 and $\frac{1}{2}k_0$ modes are stable, our theory fails for the region below the

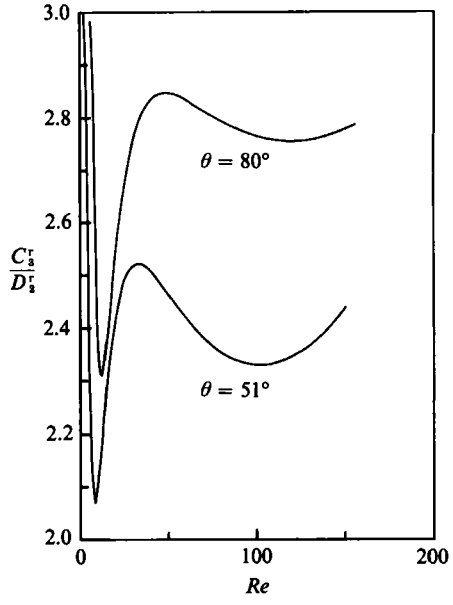

FIGURE 9. The parameter C_3^r/D_2^r which measures the bandwidth of monochromatic waves unstable to subharmonic instability. Susceptibility to subharmonic instability increases with more vertical inclines.

neutral curve for the $\frac{3}{2}$ mode. As is evident, for the region above the curve, periodic waves with wavenumbers near the neutral curve are unstable to subharmonic disturbances. In figure 9, we depict the values of C_3^r/D_2^r as functions of Re for two different inclination angles. As is consistent with figures 8 and 9, the more-vertical films have a larger band of unstable monochromatic waves and are hence more susceptible to the period-doubling phenomenon observed by Brauner & Maron (1982).

6. Conclusion

Because waves grow so rapidly in wavelength and amplitude from the inlet for high-Re films, nonlinear theories must be applied to describe them. Analysis at high Re is, however, complicated by the nonlinear inertial terms. These terms present a problem even in a linear Orr–Sommerfeld analysis. In spite of recent development in computation techniques, the fully nonlinear Navier–Stokes equation with free-surface boundary conditions is still not readily tractable. This is particularly true for solitary waves which require resolution over a large domain without the possibility of imposing periodic boundary conditions. It is hence desirable to simplify the equations of motion to reduce the computational effort. The approximate Kármán–Polhausen integral technique is introduced here for exactly this reason. Although we have shown by comparing to known results at low Re that there is a second-order error introduced by this approximation, the approximation is still a welcome one and, as we have demonstrated, provides predictions that agree with experimental data with a second-order theory. We have applied modern bifurcation techniques here to construct the long finite-amplitude waves near criticality and traced them numerically to high Reynolds numbers. The computation yields the predictions of (42) and (43) which are verified in figure 7. We have also shown that

periodic waves near the neutral curve are unstable to subharmonic instability, which supports the recent experimental observation of Brauner & Maron (1982) of the mechanism for evolution of solitary waves.

This work was partially supported by NSF contract CBT 8451116, and by ACS-PRF contract 20786-AC7. We are also grateful to Professor S.-H. Hwang for his derivation of the normal form equations.

Appendix

In this Appendix we briefly discuss the deviation of the present integral formulation from the long-wave expansion at $Re = O(1)$ and the advantages offered by the integral theory for $Re = O(\epsilon^{-1})$. For $We\,\epsilon^2 = O(1)$ and $Fr = O(1)$, a long-wave expansion of (1)–(7) of the form

$$u = u_0 + \epsilon u_1 + O(\epsilon^2), \quad v = v_0 + \epsilon v_1 + O(\epsilon^2), \quad p = p_0 + \epsilon p_1 + O(\epsilon^2) \tag{A 1}$$

yields for $Re = O(1)$ the following equations:

$$O(\epsilon^0) \quad \frac{\partial^2 u_0}{\partial y^2} = -Re\,Fr\cos\theta, \quad \frac{\partial u_0}{\partial x} + \frac{\partial v_0}{\partial y} = 0, \quad \frac{\partial p_0}{\partial y} = -Fr\sin\theta. \tag{A 2}$$

These equations can be solved with the appropriate leading-order boundary conditions to yield

$$u_0 = Fr\,Re\cos\theta(hy - \tfrac{1}{2}y^2), \tag{A 3a}$$

$$v_0 = -Fr\,Re\cos\theta h_x \tfrac{1}{2}y^2, \tag{A 3b}$$

$$p_0 = p_a - We\,\epsilon^2 h_{xx} - Fr\sin\theta(y-h). \tag{A 3c}$$

This then yields the leading-order flow rate

$$q_0 = \int_0^h u_0\,\mathrm{d}y = \tfrac{1}{3}Fr\,Re\cos\theta h^3. \tag{A 4}$$

We note by substituting (A 4) into the (A 3a) that this leading-order expression for the horizontal velocity profile is exactly that used in the integral boundary-layer theory of (16). This similarity ends, however, in the next order.

$O(\epsilon^1)$

We shall only need the horizontal velocity here,

$$\frac{\partial^2 u_1}{\partial y^2} = Re\frac{\partial p_0}{\partial x} + Re\left(\frac{\partial u_0}{\partial t} + u_0\frac{\partial u_0}{\partial x} + v_0\frac{\partial u_0}{\partial y}\right). \tag{A 5}$$

By substituting (A 3) into (A 5) and solving for u_1 with the appropriate boundary conditions, one obtains

$$u_1 = Re(We\,\epsilon^2 h_{xxx} - Fr\sin\theta h_x)(hy - \tfrac{1}{2}y^2) - Re^3 Fr^2\cos^2\theta\, h^2 h_x(\tfrac{1}{6}y^3 - \tfrac{1}{2}h^2 y) + Re^3 Fr^2\cos^2\theta h h_x(\tfrac{1}{24}y^4 - \tfrac{1}{6}h^3 y), \tag{A 6}$$

which yields the next-order flow rate

$$q_1 = \int_0^h u_1\,\mathrm{d}y = \tfrac{2}{15}Re^3 Fr^2\cos^2\theta h^6 h_x + \tfrac{1}{3}Re\,We\,\epsilon^2 h^3 h_{xxx} - \tfrac{1}{3}Re\,Fr\sin\theta h^3 h_x. \tag{A 7}$$

We note from (A 6) that the $O(\epsilon)$-resolution of the horizontal velocity profile introduces non-parabolic corrections to the parabolic profile of (A 3). This is hence

inconsistent with the approximation introduced by the integral theory, which always assumes a parabolic profile. To be more explicit, we rewrite the averaged equations, (13)–(15), to $O(\epsilon)$ in the original variables of (1)–(7) to reveal the correct order of each term,

$$\epsilon\left(\frac{\partial q}{\partial t}\right)+\epsilon\frac{\partial}{\partial x}\left(\frac{\Gamma q^2}{h}\right)=We\,\epsilon^3 hh_{xxx}+Fr(h\cos\theta-\epsilon hh_x\sin\theta)-\tau_w, \tag{A 8}$$

$$\tau_w=\frac{1}{Re}\frac{\partial u}{\partial y}(y=0)=\frac{3q}{Re\,h^2}, \tag{A 9}$$

$$\Gamma=\frac{h}{q^2}\int_0^h u^2\,dy, \tag{A 10}$$

where the assumed profile (16) has been invoked. We have solved for the waveforms of (A 8) in §§3 and 4. (Actually, a higher-order version was used.) However, one can also carry out a perturbation analysis of (A 8) for $Re = O(1)$ for comparison against the 'exact' expressions of (A 4) and (A 7) from long-wave expansion. Expanding q, Γ and τ_w,

$$q=q_0+\epsilon q_1,\quad \Gamma=\Gamma_0+\epsilon\Gamma_1,\quad \tau_w=\tau_w^0+\epsilon\tau_w^1, \tag{A 11}$$

one obtains from (A 8)–(A 10),

$$q_0=\tfrac{1}{3}Re\,Fr\,h^3\cos\theta, \tag{A 12}$$

$$q_1=\tfrac{1}{9}Re^3Fr^2\cos^2\theta h^6 h_x+\tfrac{1}{3}Re\,We\,\epsilon^2 h^3 h_{xxx}-\tfrac{1}{3}Re\,Fr\sin\theta h^3 h_x. \tag{A 13}$$

Comparing the long-wave expansion result of (A 4) and (A 7) to the integral approximation result of (A 12) and (A 13), one concludes that the assumption of a parabolic profile introduces an error in the coefficient of the first term of q_1 at low Reynolds numbers ($\frac{1}{9}$ instead of $\frac{2}{15}$). This error accounts for the factor $\frac{5}{6}$ discrepancy, which is exactly the ratio of the two coefficients in Re_c of (24). Note, however, that the functional dependence on h and its derivatives is exactly duplicated by the approximate integral theory. Consequently, the integral boundary-layer theory is correct to leading order for low Re and it introduces an error of at most 20% in the next order.

Both expansions are carried out here for $Re = O(1)$. For $Re = O(\epsilon^{-1})$, the long-wave expansions of u in (A 3a) and (A 6) are no longer valid because the nonlinear inertial terms are of the same order as the dominant viscous term. The resulting nonlinear equations at every order for the horizontal velocity such as (A 3a) and (A 5) cannot be solved explicitly. Similarly, the expansion in ϵ of the integral boundary-layer equation of (A 8) in (A 11) also yields nonlinear equations. However, instead of expanding q, one can numerically tackle the integral equation of (A 8) directly, which was carried out in this manuscript, while numerical solution of the nonlinear equations in the long-wave expansion is extremely difficult since it involves the solution of a class of equations very similar to the Navier–Stokes equation. This numerical advantage of the approximate integral theory is also the motivation behind its wide application in airfoil theory.

REFERENCES

ALEKSEENKO, S. V., NAKORYAKOV, V. YE. & POKUSAEV, B. G. 1985 Wave formation on a vertical falling liquid film. *AIChE J.* **31**, 1446–1460.

ALUKO, M. & CHANG, H.-C. 1984 PEFLOQ: An algorithm for the bifurcation analysis of periodic solutions. *Comput. Chem. Engng* **8**, 355–365.

ARMBRUSTER, D., GUCKENHEIMER, J. & HOLMES, P. 1988 Heteroclinic cycles and modulated travelling waves in systems with O(2) symmetry. *Physica* **29D**, 257–282.

BATCHELOR, G. K. 1967 *An Introduction to Fluid Dynamics*. Cambridge University Press.

BENJAMIN, T. B. 1957 Wave formation in laminar flow down an inclined plane. *J. Fluid Mech.* **2**, 554–574.

BENJAMIN, T. B. 1984 Impulse, force and variational principles. *IMA J. Appl. Maths* **32**, 3–68.

BENNEY, D. J. 1966 Long waves on liquid films. *J. Maths Phys.* **45**, 150–155.

BERTSCHY, J. R., CHIN, R. W. & ABERNATHY, F. H. 1983 High-strain-rate free-surface Boundary-layer flows. *J. Fluid Mech.* **126**, 443–461.

BRAUNER, N. 1987 Roll wave celerity and average film thickness in turbulent wavy film flow. *Chem. Engng Sci.* **42**, 265–273.

BRAUNER, N. & MARON, D. M. 1982 Characteristics of inclined thin films, waviness and the associated mass transfer. *Intl J. Heat Mass Transfer* **25**, 99–110.

BRAUNER, N. & MARON, D. M. 1983 Modelling of wavy flow in inclined thin films. *Chem. Engng Sci.* **38**, 775–788.

BROCK, R. R. 1970 Periodic permanent roll waves. *J. Hydraul. Div. ASCE* **12**, (HY), 2565–2580.

CARR, J. 1981 *Applications of Center Manifold Theory*. Springer.

CHANG, H.-C. 1987 Evolution of nonlinear waves on vertically falling films – a normal form analysis. *Chem. Engng Sci.* **42**, 515–533.

CHANG, H.-C. 1989 Onset of nonlinear waves on falling films. *Phys. Fluids* A **1**, 1314.

CHOI, I. 1977 Contributions à l'étude des mechanisms physiques de la generation des ôndes de capillarite-gravité à une interface air–eau. Thesis, Université D'Aix Marseille.

CHU, K. J. & DUKLER, A. E. 1974 Statistical characteristics of thin, wavy films: II. Studies of the substrate and its wave structure. *AICHE J.* **20**, 695–706.

CHU, K. J. & DUKLER, A. E. 1975 Statistical characteristics of thin wavy films: III. Structure of the large waves and their resistance to gas flows. *AIChE J.* **21**, 583–595.

DOEDEL, E. J. & KERNEVEZ, J. P. 1986 Software for continuation problems in ordinary differential equations with applications. *Caltech. Applied Maths Rep.*

DRESSLER, R. F. 1949 Mathematical solution of the problem of roll-waves in inclined open channels. *Commun. Pure Appl. Maths.* **2**, 149–194.

GJEVIK, B. 1970 Occurrence of finite-amplitude surface waves on falling liquid films. *Phys. Fluids* **13**, 1919–1925.

GUCKENHEIMER, J. & HOLMES, P. 1983 *Nonlinear Oscillations, Dynamical Systems and Bifurcations of Vector Fields*. Springer.

HANRATTY, T. J. 1983 In *Waves on Fluid Interfaces* (ed. R. E. Meyer), pp. 221–259. Academic.

HWANG, S.-H. & CHANG, H-C. 1987 Turbulent and inertial roll waves in inclined film flow. *Phys. Fluids* **30**, 1259–1268.

JANSSEN, P. A. E. 1986 The period-doubling of gravity–capillary waves. *J. Fluid Mech.* **172**, 531–546.

KÁRMÁN, T. VON 1921 *Z. angew. Math. Meth.* **I**, 233.

LEE, J. 1969 Kapitza's method of film flow description. *Chem. Engng Sci.* **24**, 1309–1320.

LIN, S. P. 1969 Finite amplitude stability of a parallel flow with a free surface. *J. Fluid Mech.* **36**, 113–126.

LIN, S. P. 1974 Finite-amplitude side-band instability of a viscous film. *J. Fluid Mech.* **63**, 417–429.

LIN, S. P. 1983 *Waves on Fluid Interfaces* (ed. R. E. Meyer), pp. 261–289. Academic.

NAKAYA, C. 1975 Long waves on a thin fluid layer flowing down an inclined plane. *Phys. Fluids* **18**, 1407–1420.

NAKAYA, C. 1989 Waves on a viscous fluid film down a vertical wall. *Phys. Fluids* A **1**, 1143–1154.

NEEDHAM, D. J. & MERKIN, J. H. 1984 On roll waves down an inclined channel. *Proc. R. Soc. Lond.* A **394**, 259–278.

NEEDHAM, D. J. & MERKIN, J. H. 1986 On infinite period bifurcations with an application to roll waves. *Acta Mech.* **60**, 1–16.

PUMIR, A., MANNEVILLE, P. & POMEAU, Y. 1983 On solitary waves running down an inclined plane. *J. Fluid Mech.* **135**, 27–50.

SHKADOV, V. Y. 1967 Wave conditions in the flow of thin layer of a viscous liquid under the action of gravity. *Izv. Akad. Nauk. SSSR Mekh. Zhidk. i Gaza* **1**, 43–50.

SHKADOV, V. Y. 1968 Theory of wave flows of a thin layer of viscous liquid. *Izv. Akad. Nauk. SSSr Mekh. Zhid. i Gaza* **2**, 20.

STOKER, J. J. 1957 *Water Waves.* Interscience.

YIH, C–S. 1963 Stability of liquid flow down an inclined plane. *Phys. Fluids* **6**, 321–330.

ZUFIRIA, J. A. 1987 Symmetry breaking in periodic and solitary gravity–capillary waves on water of finite depth. *J. Fluid Mech.* **184**, 183–206.